Is freeze-drying an alternative to solvent exchange for the hydration stop of cementitious suspensions?

Patrick A. Kißling [a], Franziska Lübkemann [a], Alexander Mundstock [a], Ludger Lohaus [b], Michael Haist [b], Jürgen Caro [a], Nadja C. Bigall [a,*]

[a] Institute of Physical Chemistry and Electrochemistry, Leibniz Universität Hannover, Germany
[b] Institute of Building Materials Science, Leibniz Universität Hannover, Germany

ARTICLE INFO

ABSTRACT

In order to understand the rheological properties of cementitious suspensions at early stages, among other phases, the formation of ettringite and its time-dependent influence, whether by amount or morphology, has to be examined in detail using a suitable method to stop the hydration process. It is state-of-the-art to exchange water with isopropanol, however, the water initially remains in the system possibly leading to reduced time resolution. Our group raised the question if freeze-drying or the combination of the water-isopropanol exchange with subsequent freeze-drying might be a suitable technique to achieve an almost complete hydration stop at any time. Recently, it was shown under which circumstances low-pressure characterization techniques can be employed without destroying the samples due to loss of crystal bound water. Here, by implementing these recent results, we show under which circumstances freeze-drying indeed can be employed as fast hydration stop method.

1. Introduction

In the early stages of the hydration of Portland cement, small needle-shaped crystals of ettringite are formed on the surface of cement particles, which have a noticeably impact on the suspension's rheological properties [1–7]. For a time-variant quantitative assessment of the influence of ettringite on the rheological properties, it is essential to gain knowledge about the amount of ettringite and its morphology at specific points of time during the early stage of hydration. This in turn requires a suitable method to stop the hydration process of cementitious suspensions at any possible time. In previous works by Wyrzykowski et al. [8] and Flatt et al. [9] it was stated that the reduction of relative humidity to 80% is sufficient to stop the hydration process. Here, Wyrzykowski et al. [8] showed that the hydration stop occurs under normal conditions and below a relative humidity of 80%, which takes several days (up to 10 days). The work of Flatt et al. [9] demonstrates a theoretical study of the kinetics of heat release by C_3S (alite) hydration and the evolution of ionic concentration in solution. In it, hydration stop under 80% relative humidity after a period of 90 days are shown. Here, below 80% relative humidity, the hydration stops due to negative pressure within the capillary system of the porous structure. Since our work focuses on a different time scale (up to 90 min) and the early stages of hydration, where no porous system is formed, the distinct decrease of the water content seemed to be the most reproducible way to stop the hydration. To achieve a hydration stop, it is state-of-the-art to exchange the water matrix with an organic solvent, mostly isopropanol (iPrOH) [10,11]. In some studies it was shown that it is difficult to extract the iPrOH completely from the hydration stopped sample after the solvent exchange [12–16] Alternatively, a suitable technique might be based on freezing with liquid nitrogen (LN₂) with subsequent freeze-drying [10]. Both methods possess specific advantages as well as disadvantages. The iPrOH-H₂O-exchange preserves the pore structure [17–19] but the surface of the hydrated cement is morphed, carbonate-like phases are likely to form already after an exchange time of several minutes [10,16,20], and certain hydration products are damaged [10,11,17–19,21]. The latter is due to the mechanical mixing process of the solvent exchange leading to a perturbation of the cement matrix and dehydration of ettringite [10,18,19,22]. In contrast, by submerging the cementitious

suspension in LN_2 no perturbation and thus no damage to the microstructure occurs [23–25]. It was also shown that the combination of both aforementioned techniques, meaning a gradual hydration stop by iPrOH-H_2O-exchange combined with subsequent freeze-drying, has the great potential to complement their distinct advantages, having a hydration-stopped sample whose cement matrix remained undisturbed and being completely dry [26]. Nevertheless, low pressure treatment is suspected to diminish the early stage hydration product ettringite [10,11,27–31] which is generated within the first 90 min of hydration of cement (Table S1) [7]. Based on our recent results [32] about the influence of low pressure on the crystal structure, morphology, and chemical composition of ettringite, freeze-drying as a potential hydration stop technique is further developed and optimized regarding duration and level of low-pressure treatment. Hence, all steps implementing vacuum or low pressure treatment were performed under conditions that are non-invasive to ettringite's morphological and compositional stability.

Therefore, in this work, we report on the influence of three different hydration stop techniques on cement and its hydration product ettringite to find both, the most non-invasive and complete, as well as the fastest hydration stop technique. Fig. 1 illustrates the synthesis route of the three hydration stop techniques: (1) solvent exchange with iPrOH (**Iso**), (2) freezing with LN_2 and subsequent freeze-drying (**FD**), and (3) gradual solvent exchange with iPrOH, freezing with LN_2 and subsequent freeze-drying (**IFD**). To assess changes in the crystal structures induced by these three hydration stop techniques X-ray diffraction analysis (XRD) was performed. The change in the chemical decomposition behaviour, as well as the bound water content, were evaluated by thermogravimetric analysis (TGA). As imaging technique for the morphology of the hydration-stopped and anhydrous cement particles, environmental scanning electron microscopy (ESEM) was applied. In this work, the aforementioned characterization techniques were carried out as time-dependent measurements to discuss the morphological changes at different hydration states (10 min, 30 min, 60 min, and 90 min) using three different hydration stop techniques.

2. Materials and methods

2.1. Materials

The main materials for this study were Portland cement CEM I 42.5 R from Heidelberg Cement AG (in the following referred to as cement or

CEM I), anhydrous isopropanol (≥99.95%) and anhydrous copper sulphate (≥98%) from Carl Roth, Millipore water (18.2 MΩ·cm) cleaned by an Arium 611DI from Sartorius (in the following referred to as water) and liquid nitrogen (≥99.999%) from Linde. As an internal standard for XRD measurements silicon (97.5%) from Riedel-de Haën was used. The cement was stored at ambient temperature (20 °C ± 2 °C) and humidity (18%–45%) for the whole study.

2.2. Methods

2.2.1. Cementitious suspension

Following the mixing program shown in Table 1, cementitious suspensions with a water to cement ratio w/c = 0.5 and a total volume of 500 mL were prepared. 610 g cement and 305 mL water (precooled to 10 °C) was mixed with a balloon whisk using a Kenwood KitchenAid KM336 S Chef Classic to simulate concrete mixing as usually performed at larger scales. During the first 10 min, the mixture's temperature rose to 20 °C. The last step of slow stirring at level 2 (approx. 72 rpm) was performed for different durations (6, 26, 56, and 86 min) to investigate the reaction kinetics. Afterwards, all samples were withdrawn for hydration stoppage, dried, and stored at 19.2 °C ± 0.4 °C in a dry nitrogen atmosphere for 0 to 2 d before characterization was performed.

2.2.2. Procedure for solvent exchanged samples (Iso)

After a total reaction duration of 10 min, 30 min, 60 min, and 90 min after adding water, 10 mL of the cementitious suspension were taken with an Eppendorf pipette, instantly transferred into 50 mL anhydrous isopropanol (precooled to 5 °C) in falcon tubes and agitated for 5 min at

Table 1
Mixing program for cementitious suspensions.

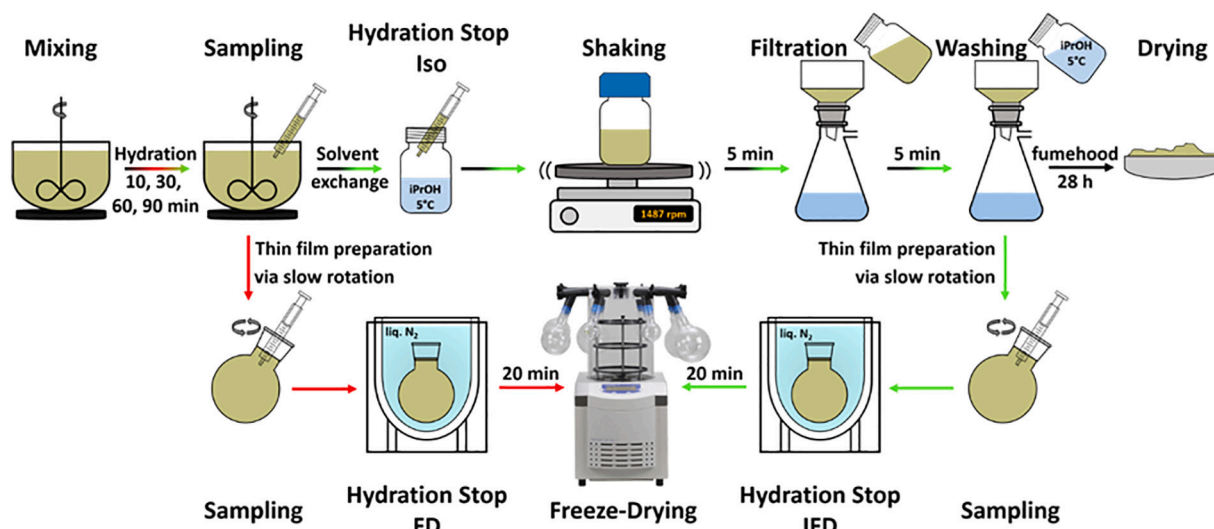| Step	Duration	Mode (Kenwood KitchenAid) [rpm]
Dry mixing of CEM I	60 s	Level 2 [approx. 72]
Adding water	30 s	Level 2 [approx. 72]
Pre-homogenisation	15 s	Level 2 [approx. 72]
Homogenisation	15 s	Maximum [approx. 220]
Stop and manually scraping off	60 s	Off
Homogenisation II	120 s	Maximum [approx. 220]
Slow stirring	Until stopped	Level 2 [approx. 72]

Fig. 1. Scheme of hydration stop by isopropanol-water exchange (**Iso**, synthesis route in black arrows), freezing with liquid nitrogen and subsequent freeze-drying (**FD**, synthesis route in red arrows), and isopropanol water exchange with subsequent freezing with liquid nitrogen and successive freeze-drying (**IFD**, synthesis route in green arrows). (For interpretation of the references to colour in this figure legend, the reader is referred to the web version of this article.)

1487 rpm with a shaker (Multi Reax by Heidolph Instruments GmbH & Co. KG), so no mechanical stirring was performed. Using a Buchner funnel the iPrOH-H_2O-suspension was filtrated using a fibreglass filter (retention 0.4 μm, MN-GF 5 by Macherey-Nagel GmbH & Co. KG). The sample was washed twice by adding 50 mL anhydrous isopropanol (precooled to 5 °C), filtrated for 5 min, and stored under ambient conditions (19.2 °C ± 0.4 °C) for 28 h in the fume hood (Fig. 1). This procedure is referred to as **Iso**. To address the possible influence of drying under ambient conditions instead of vacuum drying, five repetitions with vacuum-drying at 4 mbar for 3 h (**Iso^2**) were done and analysed by TGA.

2.2.3. Procedure for subsequent freeze-drying (FD)

After a total reaction duration of 10 min, 30 min, 60 min, and 90 min after adding water, 10 mL of the cementitious suspension were taken with an Eppendorf pipette, transferred to a 250 mL flask, which was slowly rotated to get a homogenous thin layer of cementitious suspension, and transferred quickly into LN_2 (−196.15 °C) for 20 min. Each sample was freeze-dried using a freeze-dryer (Alpha 1–2 LDplus from Martin Christ Gefriertrocknungsanlagen GmbH) coupled with a two-stage rotary vane pump (RV 12 from Edwards Vacuum) for 3 h at 4 mbar (Fig. 1). This procedure is referred to as **FD**.

2.2.4. Procedure for solvent exchanged samples with subsequent freeze-drying (IFD)

After a total reaction duration of 10 min, 30 min, 60 min, and 90 min after adding water, 10 mL of the cementitious suspension were taken with an Eppendorf pipette, instantly transferred into 50 mL anhydrous isopropanol (precooled to 5 °C) in falcon tubes and agitated for 5 min at 1487 rpm with a shaker (Multi Reax), so no mechanical stirring was performed. Using a Buchner funnel the iPrOH-H_2O-suspension was filtrated using a fibreglass filter (retention 0.4 μm). The sample was washed twice by adding 50 mL anhydrous isopropanol (precooled to 5 °C) and filtrated for 5 min. Each humid sample was transferred first into a 100 mL flask and second quickly into LN_2 for 20 min. All samples were freeze-dried using a freeze-dryer (Alpha 1–2 LDplus) coupled with a two-stage rotary vane pump (RV 12) for 3 h at 4 mbar (Fig. 1). This procedure is referred to as **IFD**.

2.2.5. Dryness test

To assess the residual water content of the samples after the hydration stop, anhydrous copper sulphate [$CuSO_4$] (up to 5 mg for freeze-dried and 50 mg up to 200 mg for solvent exchanged samples) was added to 1.0 g of the samples. If the residual water content was at least five times the molar amount of $CuSO_4$, hydration to copper sulphate pentahydrate [$CuSO_4 \cdot 5\,H_2O$] [33–37], indicated by a deep blue colour, occurred.

2.2.6. X-ray diffraction

The crystallinity was investigated by X-ray diffraction (XRD) using a Bruker D8 Advance in reflection mode. It was operated at 20 °C, 40 kV, and 40 mA using Cu-K$_\alpha$ radiation. Each measurement was done in a 2θ-range from 5° to 85°, with a step size of 0.010540856°, and 4 s per step, resulting in a total measurement time of 8.75 h. Additionally, to ensure ettringite being present, a zoom-in of the diffractogram was done in a 2θ-range from 8° to 10°, with a step size of 0.010540856°, and 12 s per step, resulting in a total measurement time of 1.62 h. The powder of each sample was transferred into an X-ray amorphous PVC powder carrier and smoothed, to avoid sample displacement. The diffraction patterns were evaluated by the database of Powder Diffraction File (PDF-2) 2020 of the International Centre for Diffraction Data (ICDD).

Furthermore, the phase ratio in anhydrous cement was evaluated by Rietveld refinement [38,39] using literature data [40–54], the measured XRD data of this work, and the software TOPASv6 by Bruker.

2.2.7. Thermogravimetric analysis

To evaluate the content of bound water (mainly from ettringite) any dried sample was investigated by thermogravimetric analysis (TGA) using a TGA/DSC 3+ from Mettler-Toledo GmbH. The samples were transferred into aluminium oxide crucibles (70 μL), before measurement. It was operated in a temperature range from 20 °C to 1100 °C under a nitrogen flow of 25 mL/min, a heating ramp of 5 K/min followed by holding the temperature at 1100 °C for 15 min. The data was normalized by mass (mg), derived once by time (s), multiplied by 3600 (for plotting in h) and plotted against temperature (°C).

Based on the results of Jakob et al. [7] dealing with the content of C-S-H and ettringite at different hydration stages, we stated that the decomposition at 130 °C ± 80 °C is attributed solely to ettringite because at this point of hydration according to observations from literature [7,57,55–57], we assume that no detectable amount of C-S-H is formed. The right shoulder of this decomposition peak could also belong to gypsum [10,58,59]. Additionally, we always compared the decomposition integral at 127.5 °C ± 17.5 °C with the integral at 445 °C ± 25 °C, which both belong to gypsum. Its ratio stayed essentially identical, so its contribution to the integral at 130 °C ± 80 °C changed only marginal. Therefore, we used the integral at 130 °C ± 80 °C for comparison of decomposition behaviour of ettringite. Nevertheless, it was recently shown by Zhang et al. [16] that after a solvent exchange with iPrOH, the solvent could not be released under normal conditions, therefore, it has to be clarified, that in the cases of **Iso** and **IFD** the first decomposition peak might be influenced by the unknown amount of chemically bound iPrOH [10].

2.2.8. Nitrogen physisorption

To assess the specific surface area and the specific volume of hydrated cement, nitrogen (N_2) physisorption was performed at a NOVA 3000e from Quantachrome GmbH & Co KG operating at 77 K. Before physisorption measurements, the samples were degassed under vacuum at 298 K for 24 h. Specific surface area and specific volume were estimated by applying the Brunauer-Emmett-Teller (BET) [60] equation. Pore volume was estimated at p/p$_0$ = 0.95345 by applying Density Functional Theory (DFT) [61,62] as well as pore size distributions by applying DFT [61,62] and Barrett-Joyner-Halenda (BJH) [63].

2.2.9. Environmental scanning electron microscopy and particle size distribution

To assess the morphology of the dried samples, environmental scanning electron microscopy (ESEM) using a Zeiss Supra VP 55, equipped with a cold field emission gun and a 4 Quadrant Backscatter Electron Detector (QBSD) was used as an imaging method. The acceleration voltage was 10 kV, the current 6 nA, and the pressure 1.0 mbar for each measurement. The powder was transferred onto an adhesive carbon disk and was cleaned from an excess sample through a compressed air gun. Each sample was degassed in the antechamber for 2.5 min for safety reasons. At a pressure of 375 nbar in the antechamber, the "Variable Pressure" mode was started. The particle size distribution for each hydration state was achieved by the evaluation of eight ESEM micrographs with a magnification of 1000 times, wherein 1000 ± 50 particles from two out of five syntheses were measured with the software ImageJ 1.52a.

2.2.10. Prolonged hydration duration

To compare the four different hydration stop techniques (**Iso** [drying under ambient conditions for 28 h in the fumehood], **Iso^2** [drying directly after filtration for 3 h @ 4 mbar], **FD**, and **IFD**) at later hydration states (9 h, 16.5 h, and 24 h) at which an appreciable amount C-S-H has formed, two repetitions were done, analysed by TGA and XRD, and evaluated. The results are shown and discussed in the Supplementary Data (Figs. S9 and S10).

3. Results and discussion

3.1. Portland cement CEM I 42.5 R

The anhydrous Portland cement CEM I 42.5 R was analysed using ESEM, TGA, and XRD to assess the state before hydration took place. ESEM micrograph (Fig. 2a) shows a non-homogeneous particle size distribution with a mean size of $d_{50} = 4.2\,\mu m \pm 0.1\,\mu m$. The TGA measurements were performed at three different heating ramps (5 K/min, 10 K/min, and 25 K/min) and the TGA spectra (Fig. 2b) show two aspects. Firstly, the usage of a steeper heating ramp leads to a decomposition slightly shifted to a higher temperature, as the system has less time to spread the thermal energy. Thus, all further TGA measurements were conducted using the lowest heating ramp of 5 K/min. Secondly, for the anhydrous cement, the following decomposition processes were identified: (1) dehydration of adsorbed water until roughly 100 °C, (2) decomposition of gypsum [$CaSO_4 \cdot 2\,H_2O$] at 127.5 °C $\pm$ 17.5 °C as well as at 445 °C $\pm$ 25 °C [10,58,59,64–66], and (3) calcite [$CaCO_3$] at 645 °C $\pm$ 125 °C [58,59,66,67].

Fig. 3 shows the diffractograms of CEM I (black), synthetic C_3S (Ca_3SiO_5, green), synthetic C_3A ($Ca_3Al_2O_6$, red) and its most prominent reflections in a range of $10° \leq 2\theta \leq 71°$ ($I_{reflection} > 0.1\,I_{max}$), which align with the literature data [40–54]. Further, the identified phases (C_3A orthorhombic, C_3A cubic, C_3S, C_2S, $CaSO_4$, C_4AF, MgO, $CaSO_4 \cdot 0.5\,H_2O$,

CaO, and SiO_2) and their ratio derived from Rietveld refinement (purple) [38,39] match the data shown by Lu et al. [68] with slight differences in their respective intensities (Fig. 3b).

3.2. Hydration stop of cementitious suspension

The hydration process of cementitious suspensions with a water to cement mass ratio of w/c = 0.5 was stopped at four defined times (10 min, 30 min, 60 min, and 90 min after the addition of water) by three different techniques (**Iso**, **FD**, and **IFD**). In order to demonstrate the reproducibility of all hydration stop techniques, five equal repetitions of the syntheses and characterisations with each analytical technique were conducted. The hydration stop enables the analysis of the cementitious suspension with slow techniques as N_2 physisorption, XRD, TGA, and ESEM to evaluate the influence of the hydration process on the chemical composition and morphology of cement. This includes information about the formation of the hydration product ettringite as well as the influence of the applied hydration stop method on the specific surface area, specific volume, porosity, crystal phases, morphology, and the content of bound water in the cementitious suspensions. To assess the possibility of further hydration processes after drying, a copper sulphate test was conducted. This test showed that in the case of solvent exchange (**Iso**), residual water was present, while methods involving freeze-drying (**FD** and **IFD**) yielded totally dry samples. Consequently, in the latter two cases further growth (after employing the hydration stop method) can be ruled out, while in the case of **Iso**, further hydration reactions might still occur.

3.2.1. Nitrogen physisorption

To gain knowledge about the anticipated changed morphology of cement grains after hydration, ad- and desorption behaviour during N_2 physisorption was examined. The isotherms (Figs. S1-S5) show small hysteresis, with varying width at different hydration durations and by different hydration stop techniques. The broadest hysteresis results from using the gradual **IFD** method. Fig. 4 summarizes the evaluation of the specific surface area (Fig. 4a), as well as specific volume (Fig. 4b), which shows a small increase for all techniques and durations of hydrated cement paste. It is noticeable that the combined technique **IFD** leads to the highest specific surface area and volume followed by **Iso** and **FD**, with a maximum after 30 min of hydration. This finding can be explained as the remaining water leads to further hydration of solvent exchanged samples (**Iso**), resulting in bigger ettringite crystals on the surface and therefore higher specific surface area and volume. The increasing specific surface area and volume itself can be explained by looking at the reaction's course. During hydration, early hydration products are formed on cement particles' surfaces, which leads to an increase of the specific surface area. It can be assumed that this process is more dominant than the agglomeration of the cement particles, which occurs simultaneously during the reaction and would possibly lead to a reduced specific surface area [69].

The pore size distribution (Fig. 5a–c) derived from N_2 physisorption measurement shows only a slight but homogenous increase of the mean pore size p_{50} relative to anhydrous cement (Fig. 5d+e). Compared to the starting material CEM I (0 min), the pore size distribution after hydration becomes broader independent of the applied hydration stop technique. This behaviour can be explained by the presence of various hydration products leading to larger surface roughness and hence to both a larger specific surface area and a larger amount of small pores.

For the sake of clarity, we note that the shown pore size distribution cannot directly be transferred to real cementitious materials, as it is most likely that the drying process leads to different pore sizes [70,71]. The reason is that during the first hours of cement hydration no robust structure occurs, which in turn conserves the pore structure during hydration. Furthermore, it can be derived that for cement samples the change of pore sizes in the nanometre range, as well as the change of surface area, is of the same order of magnitude for all three hydration
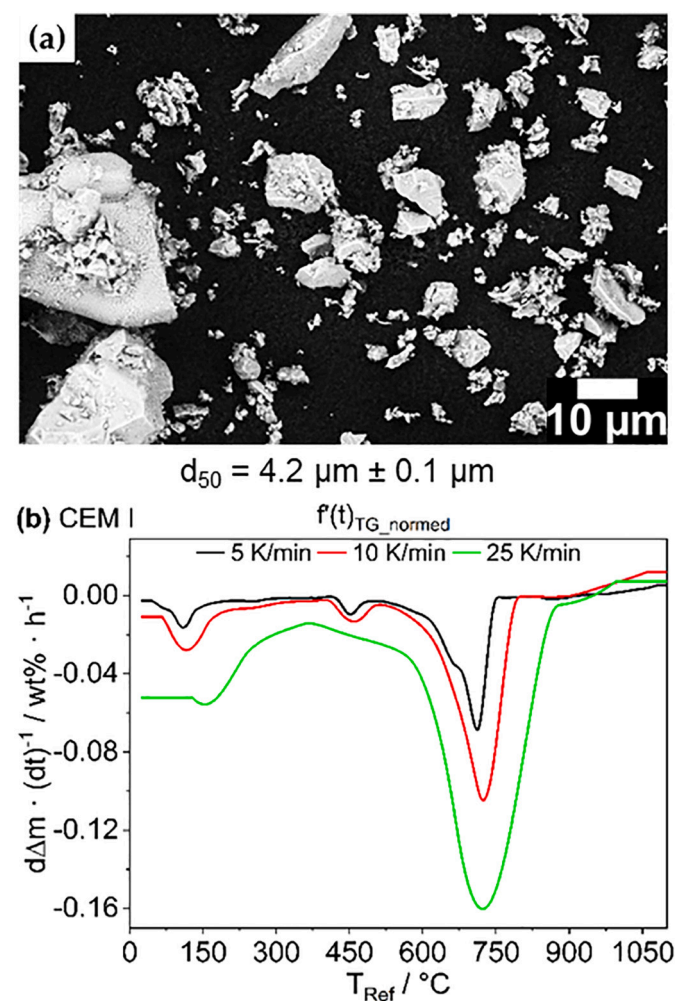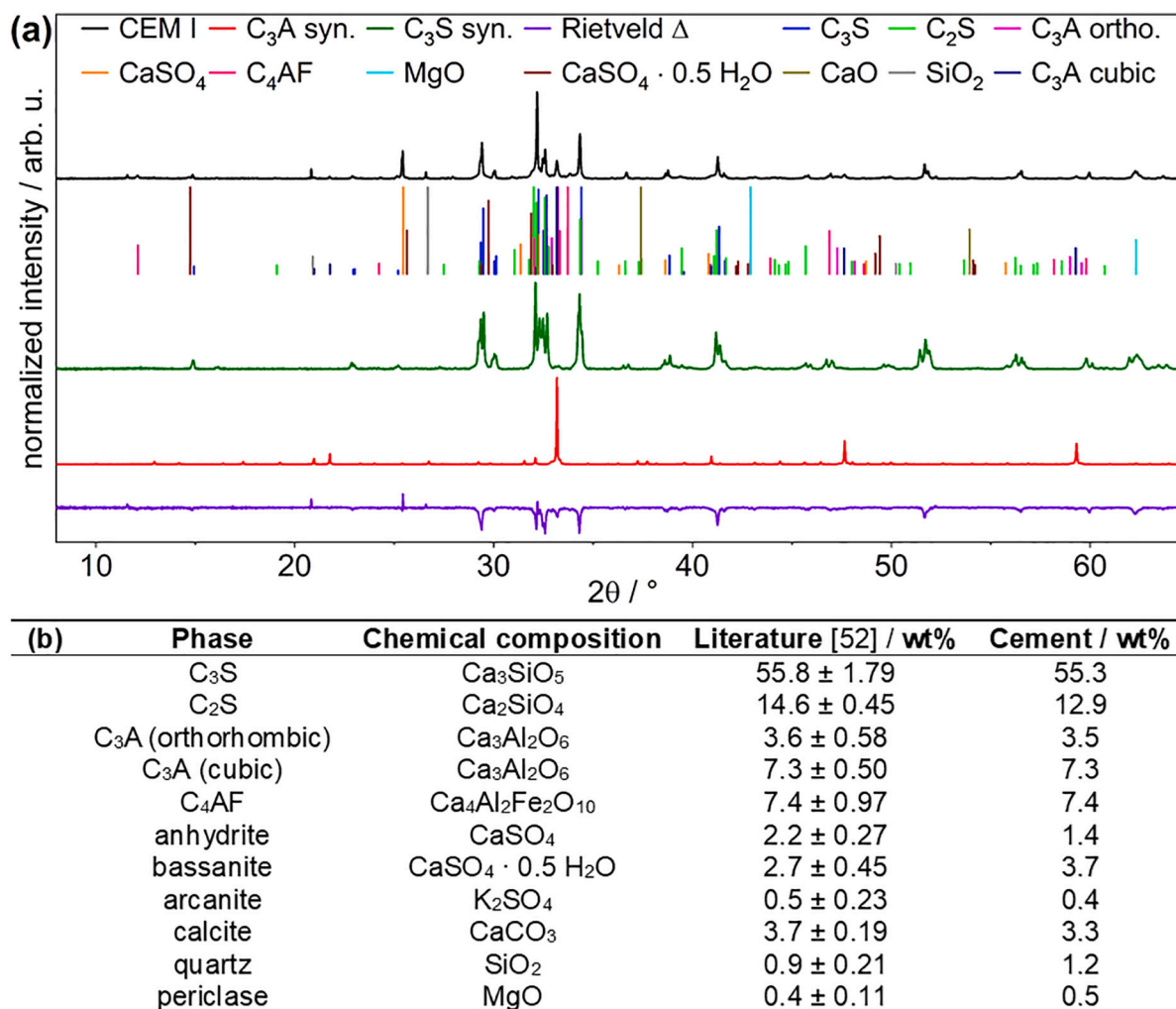

Fig. 2. (a) ESEM micrograph of anhydrous cement with mean particle size d_{50} and (b) TGA data plotted as normalized weight loss per hour against the temperature of anhydrous CEM I with different heating ramps (5 K/min, 10 K/min, and 25 K/min).

Fig. 3. (**a**) Powder X-ray diffraction pattern of anhydrous cement, its synthetic main components C₃S and C₃A, literature reflections for all identifiable phases [40–54], the result of Rietveld-Refinement indicated by difference, and (**b**) phase content of anhydrous Portland cement CEM I 42.5 R derived by Rietveld-Refinement compared to data by Lu et al. [68].

stop techniques. This indicates that all three methods indeed lead to a reaction stop.

Summarizing, evaluation of physisorption measurements showed at each specific duration and hydration stop technique the same direction of change of specific surface area, volume and pore size distribution of stopped cementitious suspensions relative to anhydrous cement. **Iso** has always the lowest value which could be an indication for the breakdown of ettringite occurring after a hydration duration of several hours [72].

3.2.2. X-ray diffraction

To link the aforementioned changes to the specific surface area, volume and pore size distribution with the presence of ettringite, XRD is employed. The diffractograms (Fig. 6) of the samples dried with the freeze-drying method (**FD**) proved their effectiveness, as all of the samples (100%, 20 of 20 measured samples), show, independent of the hydration duration, a distinct ettringite reflection in the range of $8° \leq 2\theta \leq 10°$ (Fig. 6b). Meanwhile, samples stopped by the state-of-the-art method iPrOH-H₂O-exchange (**Iso**) show a distinct (45%, 9 of 20 measured samples) and a weak noisy ettringite reflection (55%, 11 of 20 measured samples). The combination of both techniques (**IFD**) shows identical results as **Iso** (Fig. 6b).

Summarizing, the evaluation of XRD micrographs indicates that the hydration stop technique **FD** prevented the dehydration of ettringite in all 20 investigated samples, but in the case of **Iso** and **IFD** only 9 samples

(45%) had a distinct ettringite reflection. Therefore, XRD results seem to indicate that **FD** is possibly a more suited hydration stop technique to preserve ettringite, which can enable a time-variant analysis of cementitious suspensions. However, constant growth of ettringite's content in the cementitious suspensions could not be derived from the XRD data.

3.2.3. Thermogravimetric analysis

The results shown by XRD measurements are confirmed by thermogravimetric analysis (TGA) (Fig. 7). Evaluation of samples stopped by the **FD** method (Fig. 7b) shows, compared to anhydrous cement, an enhanced dehydration peak at 130 °C ± 80 °C, which aligns with preserved ettringite [32]. In contrast, the samples stopped by the **Iso** method as well as the **IFD** method show a less pronounced dehydration peak at 130 °C ± 80 °C, which is due to the lower ettringite content as also observed by aforementioned XRD investigations. The integral of this first dehydration peak varies depending on the applied hydration stop technique and hydration duration, i.e. **FD** > **Iso** > **IFD** and 90 min > 60 min > 30 min > 10 min. The anhydrous cement's degree of gypsum at 127.5 °C ± 17.5 °C and 445 °C ± 25 °C [10,58,59,64–66] as well as the content of calcite at 645 °C ± 125 °C [58,59,66,67] did not change during hydration for each applied drying technique. In case of **Iso** and **IFD** it is not possible to state that the first dehydration peak at 130 °C ± 80 °C belongs solely to ettringite because it was shown previous studies that adsorbed iPrOH is also released in this temperature range [15].
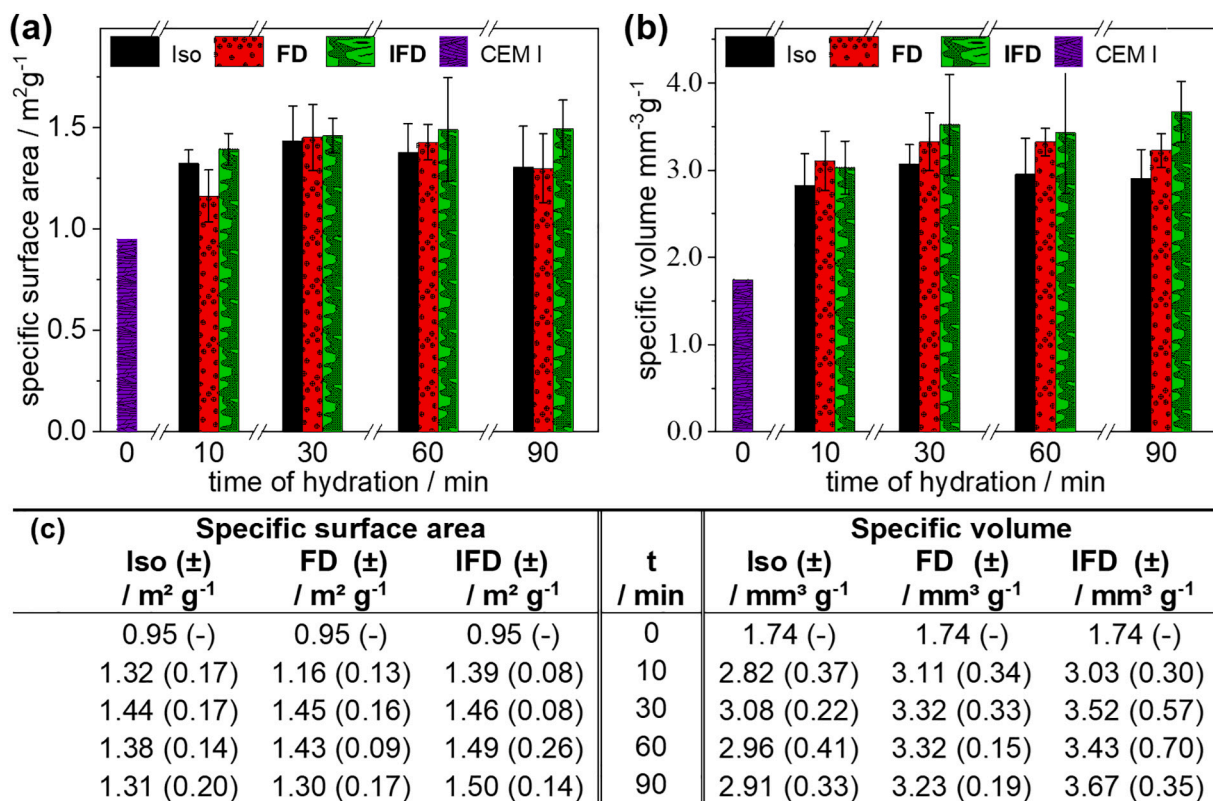
Fig. 4. N$_2$ physisorption data; (a) specific surface area, (b) specific volume of anhydrous and hydrated CEM I; stopped after various hydration durations (up to 90 min) by three different techniques (**Iso**, **FD**, and **IFD**), and (c) respective values; corresponding isotherms in Figs. S1–S5.

The table (c) values:

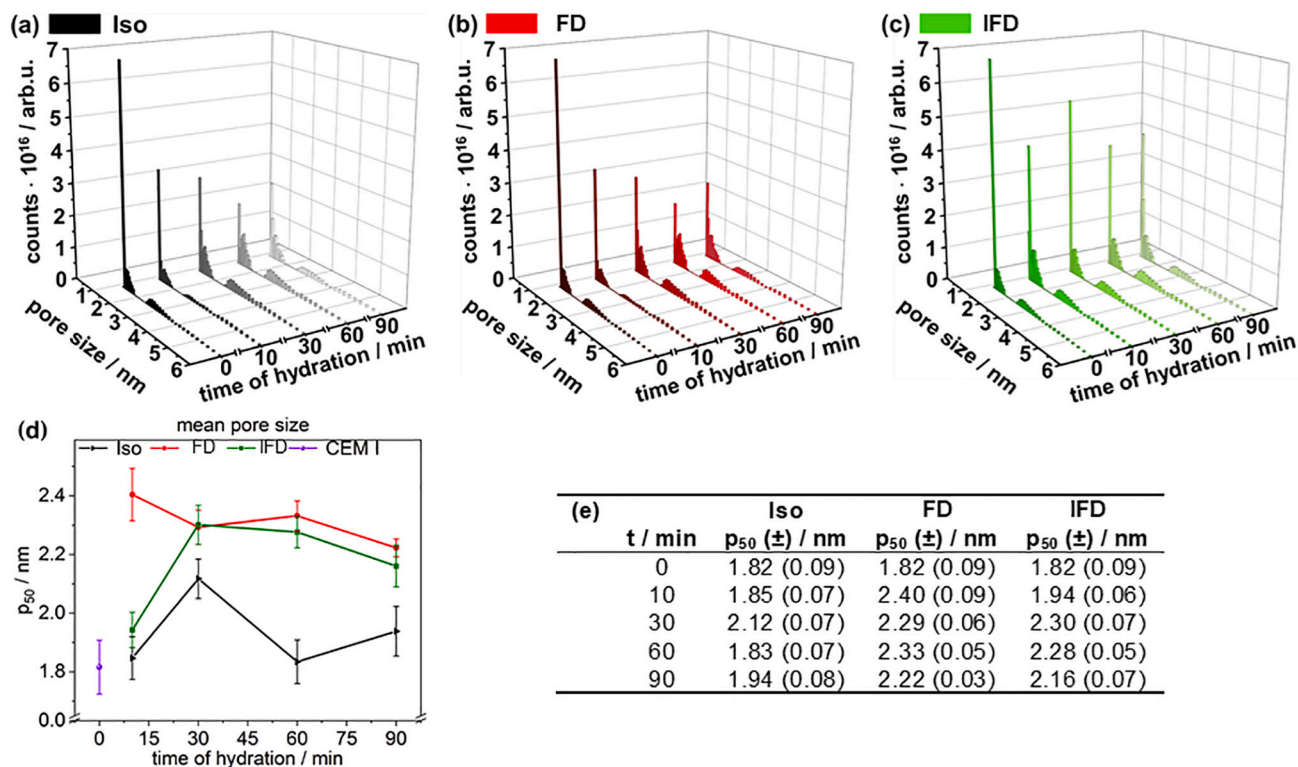| Specific surface area			t	Specific volume		
Iso (±) / m² g⁻¹	FD (±) / m² g⁻¹	IFD (±) / m² g⁻¹	/ min	Iso (±) / mm³ g⁻¹	FD (±) / mm³ g⁻¹	IFD (±) / mm³ g⁻¹
0.95 (-)	0.95 (-)	0.95 (-)	0	1.74 (-)	1.74 (-)	1.74 (-)
1.32 (0.17)	1.16 (0.13)	1.39 (0.08)	10	2.82 (0.37)	3.11 (0.34)	3.03 (0.30)
1.44 (0.17)	1.45 (0.16)	1.46 (0.08)	30	3.08 (0.22)	3.32 (0.33)	3.52 (0.57)
1.38 (0.14)	1.43 (0.09)	1.49 (0.26)	60	2.96 (0.41)	3.32 (0.15)	3.43 (0.70)
1.31 (0.20)	1.30 (0.17)	1.50 (0.14)	90	2.91 (0.33)	3.23 (0.19)	3.67 (0.35)

Fig. 5. N$_2$ physisorption measurement; pore size distribution of anhydrous and hydrated cement stopped after various hydration durations (up to 90 min) by three different techniques (**a**) **Iso**, (b) **FD**, and (**c**) **IFD**, (**d**) mean pore size p_{50} of anhydrous and hydrated cement, and (**e**) corresponding mean values.

Table (e):

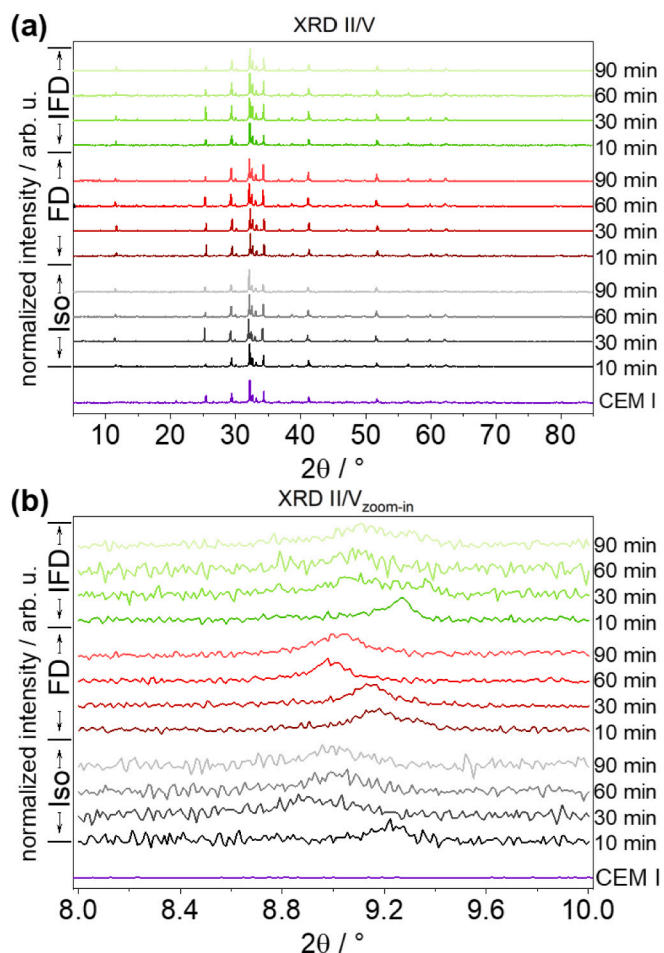| t / min	Iso p_{50} (±) / nm	FD p_{50} (±) / nm	IFD p_{50} (±) / nm
0	1.82 (0.09)	1.82 (0.09)	1.82 (0.09)
10	1.85 (0.07)	2.40 (0.09)	1.94 (0.06)
30	2.12 (0.07)	2.29 (0.06)	2.30 (0.07)
60	1.83 (0.07)	2.33 (0.05)	2.28 (0.05)
90	1.94 (0.08)	2.22 (0.03)	2.16 (0.07)

Fig. 6. Powder X-ray diffraction patterns of anhydrous and hydrated CEM I stopped after various hydration durations (up to 90 min) by three different techniques (**Iso**, **FD**, and **IFD**) in an angle range of (**a**) $5° \leq 2\theta \leq 85°$ and (**b**) of $8° \leq 2\theta \leq 10°$; complete overview in Fig. S6.

Fig. 7. TGA data plotted as mass normalized time derived weight loss ($d\Delta m \cdot (dt)^{-1}$) per hour against the reference temperature of anhydrous and hydrated CEM I with a heating rate of 5 K/min; stopped after various hydration durations (up to 90 min) by three different techniques (**a**) **Iso**, (**b**) **FD**, and (**c**) **IFD**; complete overview in Fig. S7.

Additionally, Trenwith [73] showed the decomposition of iPrOH being at 488 °C ± 40 °C, however, within the present work the described process has no significant influence in this temperature range.

These findings suggest that freeze-drying retains the highest amount of ettringite, which aligns with XRD results. Furthermore, **FD** has the advantage that one parameter less has to be considered, as in the proposed **FD** technique no solvent exchange is needed. Therefore, freeze-drying **FD** seems to be superior to or at least on par with the state-of-the-art iPrOH-H$_2$O-exchange technique **Iso** and the combined iPrOH-H$_2$O-exchange freeze-drying technique **IFD**.

To assess the influence of the drying technique after isopropanol-water exchange, two types of drying, (1) under ambient conditions (19.2 °C ± 0.4 °C) for 28 h in the fume hood (**Iso**) and (2) vacuum drying at 4 mbar for 3 h (**Iso^2**) were implemented and analysed by TGA (Fig. 8). Both techniques point to the same result that at this early stage of hydration no influence of the applied drying technique is distinguishable. The evaluation by TGA shows that the main decomposition peak of ettringite at 130 °C ± 80 °C has nearly the same topology for both solvent exchange-based hydration stop techniques (**Iso^2** and **Iso**). Differences are slightly visible at 445 °C ± 25 °C belonging to gypsum [10,58,59,66,64–66] and more distinguishable at 645 °C ± 125 °C, wherein at hydration stages (up to 60 min) the integral of samples stopped by **Iso^2** are steeper, indicating a higher amount of calcite [58,59,66,67] in these samples. Therefore, in our opinion the used drying under ambient conditions (**Iso**) is as applicable as vacuum drying at 4 mbar for 3 h or even better suited at these early hydration states.
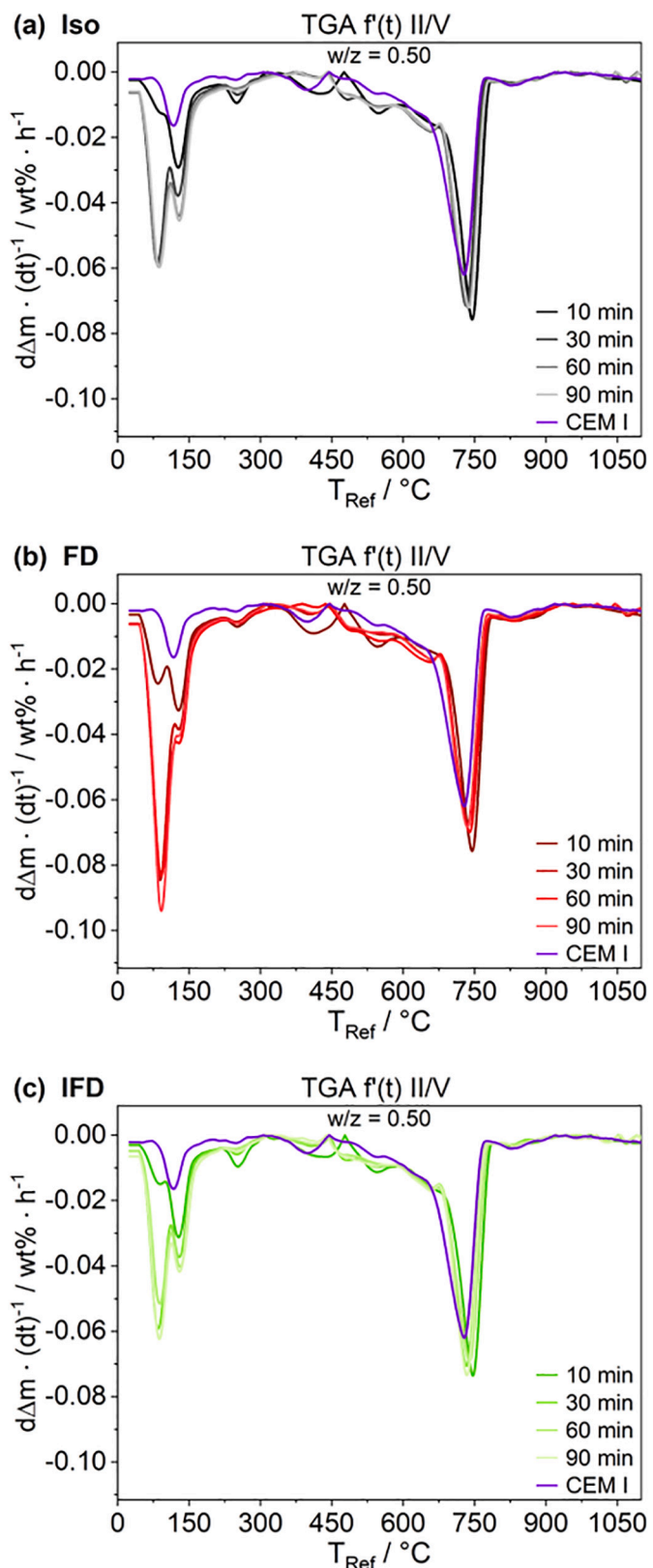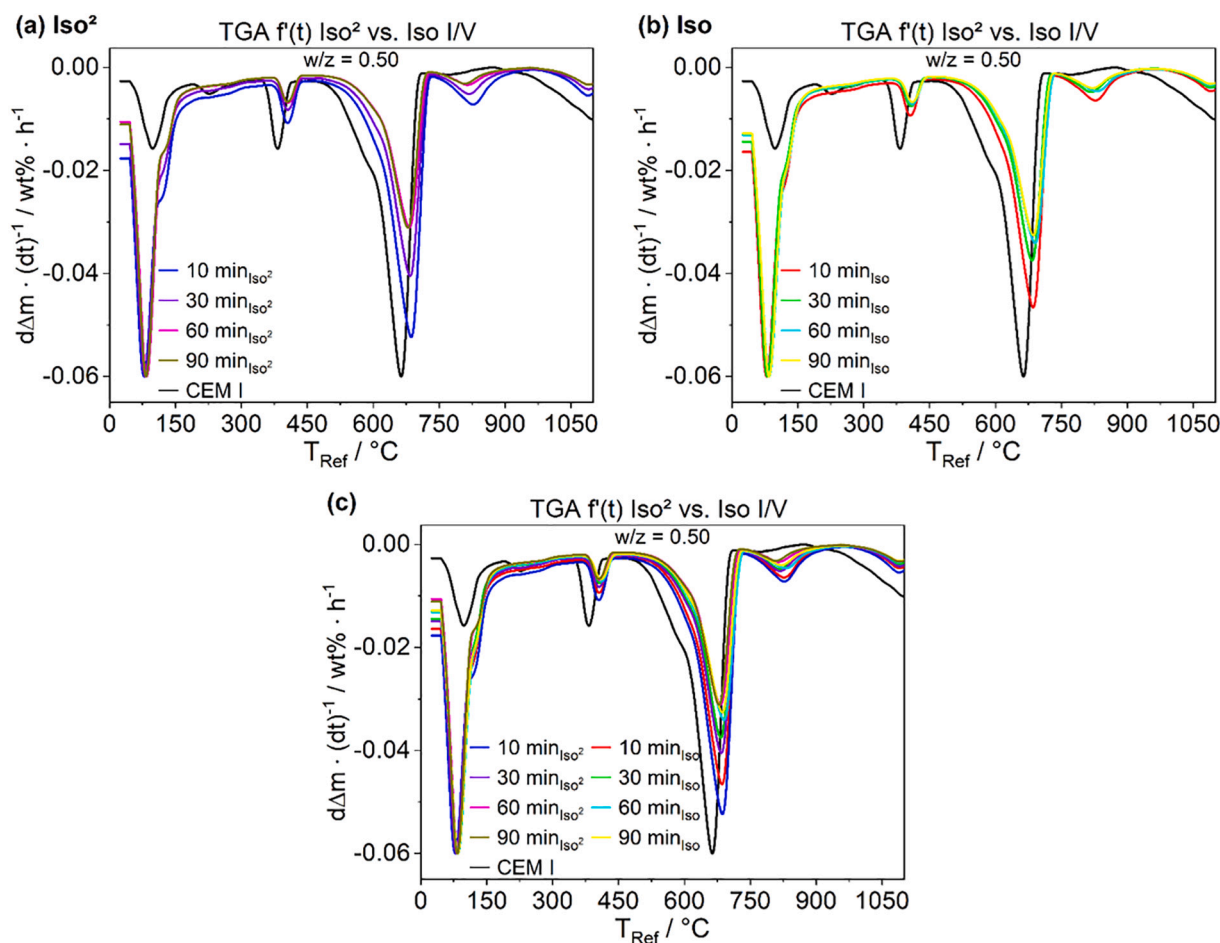
Fig. 8. TGA data plotted as mass normalized time derived weight loss $(d\Delta m \cdot (dt)^{-1})$ per hour against the reference temperature of anhydrous and hydrated CEM I with a heating rate of 5 K/min; stopped after various hydration durations (up to 90 min) **Iso** and **Iso²**; (**a**) **Iso²**, (**b**) **Iso**, and (**c**) direct overlay; complete overview in Fig. S8.

3.2.4. Environmental scanning electron microscopy

Finally, to visualize the particles' morphology and texture environmental scanning electron microscopy (ESEM) was employed (Fig. 9). Their visual reproducibility was verified by taking micrographs of different syntheses of the same hydration state. It is noticeably that after different hydration durations (up to 90 min) independent of the applied hydration stop technique (**Iso, FD,** and **IFD**) the particles are non-homogenously distributed, but a higher amount of small particles, relative to anhydrous cement (Fig. 2a), is detectable. The surfaces of the bigger particles seem to be less rough, leading to the assumption that these are non-reacted C_3S particles, as the hydration process of C_3S starts only after several hours [6,10,74–76].

Additionally, based on the ESEM micrographs, particle size distributions, as well as mean particle sizes, were evaluated (Fig. 10). Differences in the distribution of the particles, independent of the hydration stop technique applied, are marginal (Fig. 10a–c). The mean particle size (Fig. 10d+e) of freeze-dried samples (**FD**) decreases by 17% (from 4.21 μm to 3.49 μm, 0.83 $d_{50, CEM I}$) over the first 10 min, rises slightly by 6% (from 3.49 μm to 3.69 μm, 0.88 $d_{50, CEM I}$) to its maximum after 30 min of hydration, whereby the longest hydration duration of 90 min shows the smallest particles (2.99 μm, 0.71 $d_{50, CEM I}$). Solvent exchange (**Iso**) leads to a similar decrease by 20% (from 4.21 μm to 3.30 μm, 0.80 $d_{50, CEM I}$) over the first 10 min of hydration, rises by 18% (from 3.30 μm to 3.97 μm, 0.94 $d_{50, CEM I}$), decreases again by 7% (from 3.97 μm to 3.68 μm, 0.87 $d_{50, CEM I}$) and reaches its maximal particle size after 90 min (4.27 μm, 1.01 $d_{50, CEM I}$). The combination of both techniques (**IFD**) shows a less pronounced decrease by 12% (from 4.21 μm to 3.69 μm, 0.88 $d_{50,}$ $_{CEM I}$) over the first 10 min, rises by 15% (from 3.69 μm to 4.25 μm, 1.01 $d_{50, CEM I}$) after 30 min and 60 min (4.20 μm), before a decay of 13% (from 4.20 μm to 3.67 μm, 0.87 $d_{50, CEM I}$) is visible. The stagnating growth could be explained as at the dormant stage, which has been reported to be between 30 min and 90 min [69], the hydration kinetics are reduced, which in turn means that the forming of hydration products on the surface of cement particles is in equilibrium with the agglomeration of the cement particles. After a short hydration period of 10 min, freeze-dried samples show a slightly higher d_{50}-value compared to samples treated with isopropanol (**Iso** and **IFD**). Although, the following hydration period shows larger particle sizes for solvent exchanged samples (**Iso** and **IFD**). The larger particles could be, as previously hypothesized [26], identified as agglomerations of smaller particles induced by iPrOH treatment, although the difference is less concise.

In summary, the imaging technique ESEM reveals, dependent on the applied hydration stop technique (**Iso, FD,** and **IFD**), small differences in the respective particle size distribution, and ESEM reveals growing particles with longer hydration duration and points out that solvent exchange with iPrOH leads to enlarged particles.

4. Conclusions

The method used to stop the hydration of cementitious suspensions, namely freeze-drying of samples frozen in liquid nitrogen (**FD**), solvent exchange with isopropanol (**Iso**), and solvent exchange with subsequent freeze-drying (**IFD**), has an impact on the mineralogical composition as well as the morphology of hydrated Portland cement (CEM I 42.5 R). It
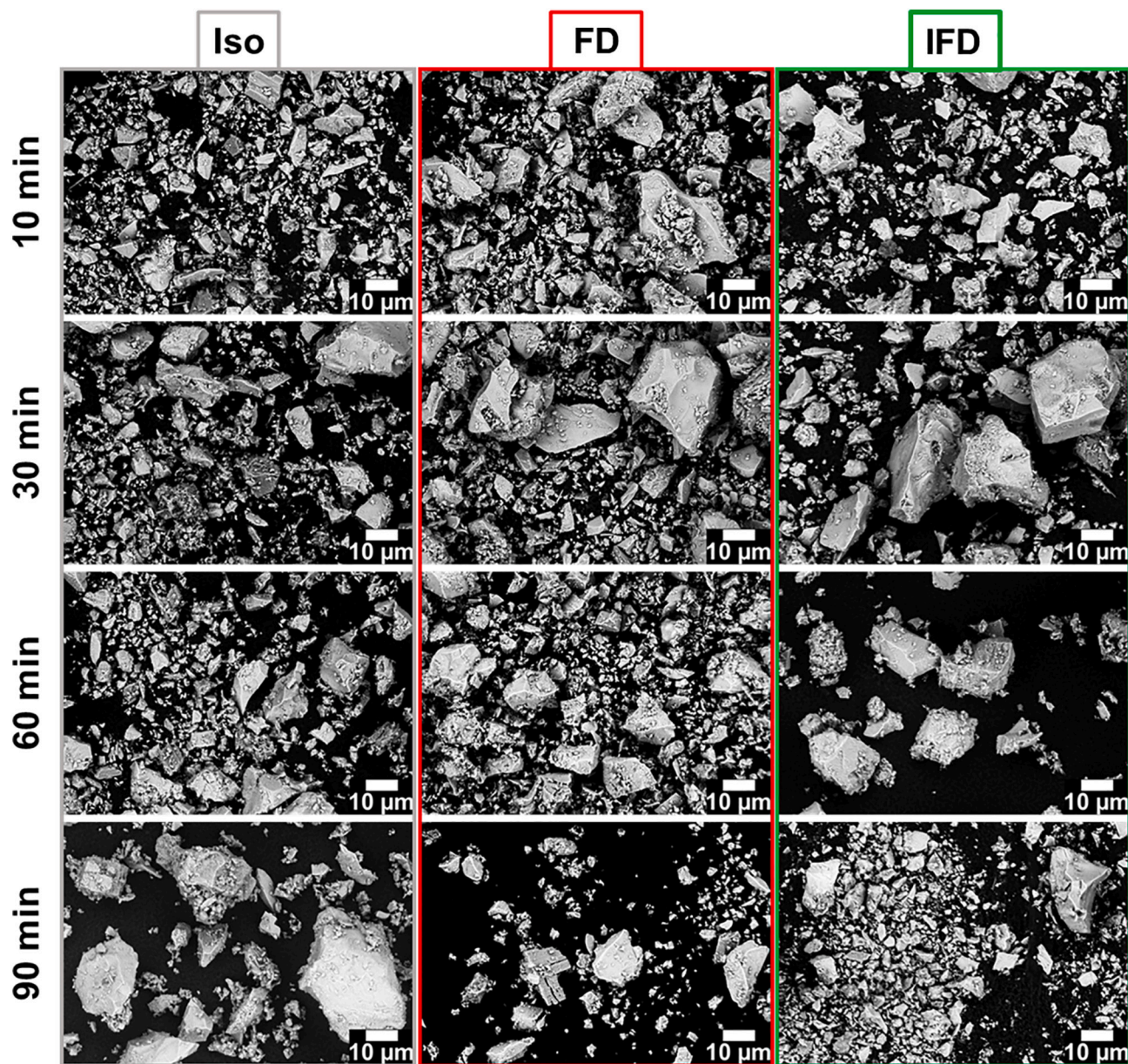
Fig. 9. ESEM micrographs of hydrated cement stopped after various hydration durations (up to 90 min) by three different techniques (**Iso**, **FD**, and **IFD**); 1.0 mbar, 6 nA, and 10 kV.

was shown by X-Ray diffraction (XRD) and thermogravimetric analysis (TGA) that the technique **FD** preserves the highest amount of ettringite at every hydration stage (10 min, 30 min, 60 min, and 90 min). Methods using solvent exchange with isopropanol (**Iso** and **IFD**) lead to an inconsistent degree of ettringite at the aforementioned hydration stages. These results are supported by nitrogen physisorption measurements of treated samples, wherein the specific surface area and the volume indicate the growth of ettringite. Noteworthy, **Iso** and **IFD** show their respective maxima earlier compared to **FD**. This can be explained by the fact that the use of **Iso** has the disadvantage that after the solvent exchange the samples are not water-free, which in turn might lead to further hydration of the cementitious suspension as well as undermines the idea of a time-variant analysis since it is not known in which hydration state the sample was stopped. The particle size distribution derived from environmental scanning electron microscopy (ESEM) showed only a slight change compared to anhydrous cement. Nevertheless, ESEM depicts, dependent on the applied hydration stop technique (**Iso**, **FD** and **IFD**), small differences in the respective particle size

distribution, shows growing particles with longer hydration duration, and points out that solvent exchange with iPrOH leads to enlarged particles.

The freeze-drying technique (**FD**) shown in this article was optimized to the point that it is a suitable technique to stop the hydration process of cementitious suspensions nearly instantly without disturbing the cement matrix, damaging or morphing the surface of hydrated cement, as well as without changes to the chemical composition e.g. formation carbonate-like phases. The freeze-drying technique (**FD**) enables the hydration to be stopped completely after defined hydration durations, enabling a precise time-variant analysis of the hydrated cement. The proposed freeze-drying technique (**FD**) allows compared to **Iso** and **IFD** the preparation of more reproducible samples and further, has the advantage that one parameter less has to be considered as no solvent exchange is needed. Therefore, freeze-drying (**FD**) seems to be a superior alternative to the state-of-the-art method, solvent exchange with isopropanol (**Iso**).

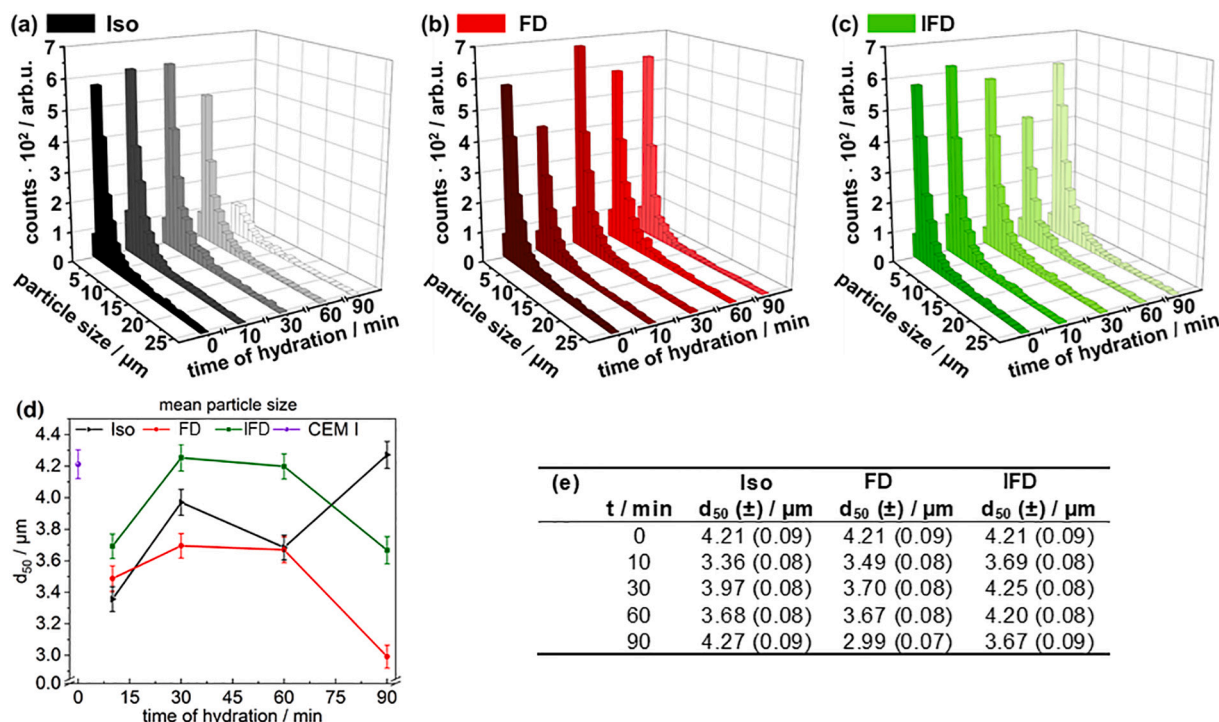Supplementary data to this article can be found online at https://doi.

Fig. 10. Particle size distribution of anhydrous and hydrated cement derived from ESEM micrographs, stopped after various hydration durations (up to 90 min) by three different techniques, (**a**) **Iso**, (**b**) **FD**, and (**c**) **IFD**, and (**d**) corresponding mean particle size d_{50}, and (**e**) mean values.

org/10.1016/j.cemconres.2022.106841.

CRediT authorship contribution statement

Patrick A. Kißling: Conceptualization, XRD, TGA, BET, Formal analysis, Validation, Investigation, Data curation, Writing – original draft, Writing – review & editing, Visualization.
Franziska Lükemann: Writing – review & editing.
Alexander Mundstock: Writing – review & editing.
Ludger Lohaus: Resources, Writing – review & editing.
Jürgen Caro: Writing – review & editing.
Michael Haist: Writing – review & editing.
Nadja C. Bigall: Conceptualization, Resources, Writing – review & editing, Supervision, Funding acquisition.

Declaration of competing interest

The authors declare that they have no known competing financial interests or personal relationships that could have appeared to influence the work reported in this paper.

Acknowledgements

References

[1] F. Winnefeld, A. Zingg, L. Holzer, J. Pakusch, S. Becker, The ettringite-superplasticizer interaction and its impact on ettringite distribution in cement suspensions, in: 9th ACI Int. Conf. Superplast. Other Chem. Admixtures Concr. Sevilla, Spain, Oct. 12-14, 2009, Sevilla, Spain, 2009, pp. 420.1–420.17.
[2] G.H. Tattersall, Workability And Quality Control of Concrete, 1st ed., CRC Press, London, 2014 https://doi.org/10.1201/9781482267006.
[3] J. Gołaszewski, Influence of cement properties on rheology of fresh cement mortars without and with superplasticizer, Archit. Civ. Eng. Environ. 4 (2008) 49–66.
[4] L.J. Struble, W.-G. Lei, Rheological changes associated with setting of cement paste, Adv. Cem. Based Mater. 2 (1995) 224–230, https://doi.org/10.1016/1065-7355(95)90041-1.
[5] H. Uchikawa, K. Ogawa, S. Uchida, Influence of character of clinker on the early hydration process and rheological property of cement paste, Cem. Concr. Res. 15 (1985) 561–572, https://doi.org/10.1016/0008-8846(85)90053-5.
[6] U. Pott, C. Ehm, C. Jakob, D. Stephan, in: Investigation of the Early Cement Hydration With a New Penetration Test, Rheometry And In-situ XRD, 2020, pp. 246–255, https://doi.org/10.1007/978-3-030-22566-7_29.
[7] C. Jakob, D. Jansen, N. Ukrainczyk, E. Koenders, U. Pott, D. Stephan, J. Neubauer, Relating ettringite formation and rheological changes during the initial cement hydration: a comparative study applying XRD analysis, rheological measurements and modeling, Materials (Basel) 12 (2019) 2957, https://doi.org/10.3390/ma12182957.
[8] M. Wyrzykowski, P. Lura, Effect of relative humidity decrease due to self-desiccation on the hydration kinetics of cement, Cem. Concr. Res. 85 (2016) 75–81, https://doi.org/10.1016/j.cemconres.2016.04.003.
[9] R.J. Flatt, G.W. Scherer, J.W. Bullard, Why alite stops hydrating below 80% relative humidity, Cem. Concr. Res. 41 (2011) 987–992, https://doi.org/10.1016/j.cemconres.2011.06.001.
[10] K. Scrivener, R. Snellings, B. Lothenbach, A Practical Guide to Microstructural Analysis of Cementitious Materials, CRC PR INC, 2015 (22. Dezember 2015).
[11] J.M. Makar, T. Sato, The effect of drying method on ordinary Portland cement surfaces during the early stages of hydration, Mater. Struct. Constr. 46 (2013) 1–12, https://doi.org/10.1617/s11527-012-9878-2.
[12] D.C. Hughes, The use of solvent exchange to monitor diffusion characteristics of cement pastes containing silica fume, Cem. Concr. Res. 18 (1988) 321–324, https://doi.org/10.1016/0008-8846(88)90016-6.
[13] D.C. Hughes, N.L. Crossley, Pore structure characterisation of GGBS/OPC grouts using solvent techniques, Cem. Concr. Res. 24 (1994) 1255–1266, https://doi.org/10.1016/0008-8846(94)90110-4.
[14] H.F.W. Taylor, A.B. Turner, Reactions of tricalcium silicate paste with organic liquids, Cem. Concr. Res. 17 (1987) 613–623.
[15] Z. Zhang, G.W. Scherer, Evaluation of drying methods by nitrogen adsorption, Cem. Concr. Res. 120 (2019) 13–26, https://doi.org/10.1016/j.cemconres.2019.02.016.

[16] G.W. Zhang, Scherer, physical and chemical effects of isopropanol exchange in cement-based materials, Cem. Concr. Res. 145 (2021), 106461, https://doi.org/10.1016/j.cemconres.2021.106461.

[17] V. Kocaba, Development And Evaluation of Methods to Follow Microstructural Development of Cementitious Systems Including Slags, École Polytechnique Fédérale de Lausanne, 2009.

[18] S. Mantellato, M. Palacios, R.J. Flatt, Reliable specific surface area measurements on anhydrous cements, Cem. Concr. Res. 67 (2015) 286–291, https://doi.org/10.1016/j.cemconres.2014.10.009.

[19] S. Mantellato, M. Palacios, R.J. Flatt, Impact of sample preparation on the specific surface area of synthetic ettringite, Cem. Concr. Res. 86 (2016) 20–28, https://doi.org/10.1016/j.cemconres.2016.04.005.

[20] L.D. Mitchell, J.C. Margeson, The effects of solvents on C-S-H as determined by thermal analysis, J. Therm. Anal. Calorim. 86 (2006) 591–594, https://doi.org/10.1007/s10973-006-7712-1.

[21] A. Mezhov, D. Kulisch, A. Goncharov, S. Zhutovsky, in: Effect of Soaking Time in a Solvent on Hydration Stoppage of Cement, 2020, pp. 23–27, https://doi.org/10.1007/978-3-030-43332-1_5.

[22] V. Kocaba, E. Gallucci, K.L. Scrivener, Methods for determination of degree of reaction of slag in blended cement pastes, Cem. Concr. Res. 42 (2012) 511–525, https://doi.org/10.1016/j.cemconres.2011.11.010.

[23] C. Gallé, Effect of drying on cement-based materials pore structure as identified by mercury intrusion porosimetry, Cem. Concr. Res. 31 (2001) 1467–1477, https://doi.org/10.1016/S0008-8846(01)00594-4.

[24] M. Moukwa, P.C. Aitcin, The effect of drying on cement pastes pore structure as determined by mercury porosimetry, Cem. Concr. Res. 18 (1988) 745–752, https://doi.org/10.1016/0008-8846(88)90090-1.

[25] A. Zingg, L. Holzer, A. Kaech, F. Winnefeld, J. Pakusch, S. Becker, L. Gauckler, The microstructure of dispersed and non-dispersed fresh cement pastes - new insight by cryo-microscopy, Cem. Concr. Res. 38 (2008) 522–529, https://doi.org/10.1016/j.cemconres.2007.11.007.

[26] P.A. Kißling, D. Cotardo, T. von Bronk, L. Lohaus, N.C. Bigall, Comparison of water-isopropanol replacement and lyophilisation for hydration stop of cementitious suspensions, in: V. Mechtcherine, K. Khayat, E. Secrieru (Eds.), Rheol. Process. Constr. Mater. RheoCon 2019, SCC 2019, Springer, Cham, 2020, pp. 610–618, https://doi.org/10.1007/978-3-030-22566-7_71.

[27] J. Marchand, R. Pleau, R. Gagné, Deterioration of concrete due to freezing and thawing, in: Mater. Sci. Concr Vol. IV, 1995, pp. 283–354.

[28] R.L. Day, B.K. Marsh, Measurement of porosity in blended cement pastes, Cem. Concr. Res. 18 (1988) 63–73, https://doi.org/10.1016/0008-8846(88)90122-6.

[29] N.N. Skoblinskaya, K.G. Krasilnikov, Changes in crystal structure of ettringite on dehydration. 1, Cem. Concr. Res. 5 (1975) 381–394.

[30] N.N. Skoblinskaya, K.G. Krasilnikov, L.V. Nikitina, V.P. Varlamov, Changes in crystal structure of ettringite on dehydration. 2, Cem. Concr. Res. 5 (1975) 419–431, https://doi.org/10.1016/0008-8846(75)90017-4.

[31] R. Snellings, J. Chwast, Ö. Cizer, N. De Belie, Y. Dhandapani, P. Durdzinski, J. Elsen, J. Haufe, D. Hooton, C. Patapy, M. Santhanam, K. Scrivener, D. Snoeck, L. Steger, S. Tongbo, A. Vollpracht, F. Winnefeld, B. Lothenbach, Report of TC 238-SCM: hydration stoppage methods for phase assemblage studies of blended cements—results of a round robin test, Mater. Struct. Constr. 51 (2018), https://doi.org/10.1617/s11527-018-1237-5.

[32] P.A. Kißling, F. Lübkemann, T. von Bronk, D. Cotardo, L. Lei, A. Feldhoff, L. Lohaus, M. Haist, N.C. Bigall, Influence of low-pressure treatment on the morphology and compositional stability of microscopic ettringite, Materials (Basel) 14 (2021) 2720, https://doi.org/10.3390/ma14112720.

[33] H. Bannwarth, B.P. Kremer, Vom Stoffaufbau zum Stoffwechsel, 2007.

[34] K. Bernhauer, Einführung in die organisch-chemische Laboratoriumstechnik, Springer Berlin Heidelberg, Berlin,Heidelberg, 1942, https://doi.org/10.1007/978-3-662-02148-4.

[35] J. Houben, Die Methoden der Organischen Chemie, 3rd ed., Georg Thieme Verlag, Stuttgart, 1925 https://doi.org/10.1055/b-003-125733.

[36] A. Stähler, Handbuch der Arbeitsmethoden in der anorganischen Chemie, Walter de Gruyter, Berlin, 1913.

[37] T. Wieland, L. Gattermann, Die Praxis des organischen Chemikers, De Gruyter, Berlin,Boston, 1952, https://doi.org/10.1515/9783111722535.

[38] H.M. Rietveld, A profile refinement method for nuclear and magnetic structures, J. Appl. Crystallogr. 2 (1969) 65–71, https://doi.org/10.1107/S0021889869006558.

[39] P. Paufler, R.A. Young (Eds.), The Rietveld Method. International Union of Crystallography, Oxford University Press, 1993, 298 p. Price £ 45.00. ISBN 0–19–855577–6, Cryst. Res. Technol. 30 (1995) 494–494. doi:10.1002/crat.2170300412.

[40] Á.G. De La Torre, S. Bruque, J. Campo, M.A.G. Aranda, The superstructure of C3S from synchrotron and neutron powder diffraction and its role in quantitative phase analyses, Cem. Concr. Res. 32 (2002) 1347–1356, https://doi.org/10.1016/S0008-8846(02)00796-2.

[41] F.C. Hawthorne, R.B. Ferguson, Anhydrous sulfates II. Refinement of the crystal structure of anhydrite, Can. Mineral. 13 (1975) 289–292.

[42] L. Desgranges, D. Grebille, G. Calvarin, G. Chevrier, N. Floquet, J.-C. Niepce, Hydrogen thermal motion in calcium hydroxide: Ca(OH)2, Acta Crystallogr. Sect. B 49 (1993) 812–817, https://doi.org/10.1107/S0108768193003556.

[43] G.A. Lager, J.D. Jorgensen, F.J. Rotella, Crystal structure and thermal expansion of a-quartz SiO2 at low temperatures, J. Appl. Phys. 53 (1982) 6751–6756, https://doi.org/10.1063/1.330062.

[44] M.R. Hartman, R. Berliner, Investigation of the structure of ettringite by time-of-flight neutron powder diffraction techniques, Cem. Concr. Res. 36 (2006) 364–370, https://doi.org/10.1016/j.cemconres.2005.08.004.

[45] M.I. McCarthy, N.M. Harrison, Ab initio determination of the bulk properties of MgO, Phys. Rev. B 49 (1994) 8574–8582, https://doi.org/10.1103/PhysRevB.49.8574.

[46] T. Pilati, F. Demartin, C.M. Gramaccioli, Lattice-dynamical estimation of atomic displacement parameters in carbonates: calcite and aragonite CaCO3, dolomite CaMg(CO3)2 and magnesite MgCO3, Acta Crystallogr. Sect. B Struct. Sci. 54 (1998) 515–523, https://doi.org/10.1107/S0108768197018181.

[47] J.A. McGinnety, Redetermination of the structures of potassium sulphate and potassium chromate: the effect of electrostatic crystal forces upon observed bond lengths, Acta Crystallogr.Sect. B Struct. Crystallogr. Cryst. Chem. 28 (1972) 2845–2852, https://doi.org/10.1107/s0567740872007022.

[48] C. Bezou, A. Nonat, J.-C. Mutin, A.N. Christensen, M.S. Lehmann, Investigation of the crystal structure of -CaSO4, CaSO4 · 0.5 H2O, and CaSO4 · 0.6 H2O by powder diffraction methods, J. Solid State Chem. 117 (1995) 165–176, https://doi.org/10.1006/jssc.1995.1260.

[49] W. Mumme, R. Hill, G. Bushnellwye, E. Segnit, Rietveld crystal structure refinements, crystal chemistry and calculated powder diffraction data for the polymorphs of dicalcium silicate and related phases, NEUES Jahrb.Mineral. 169 (1995) 35–68, http://hdl.handle.net/102.100.100/230393?index=1, http://hdl.handle.net/102.100.100/230393?index=1.

[50] P. Mondal, J.W. Jeffery, The crystal structure of tricalcium aluminate, Ca3Al2O6, Acta Crystallogr.Sect. B Struct. Crystallogr. Cryst. Chem. 31 (1975) 689–697, https://doi.org/10.1107/S0567740875003639.

[51] F. Nishi, Y. Takéuchi, The Al6O18 rings of tetrahedra in the structure of Ca8.5NaAl6O18, Acta Crystallogr.Sect. B Struct. Crystallogr. Cryst. Chem. 31 (1975) 1169–1173, https://doi.org/10.1107/S0567740875004736.

[52] A.A. Colville, S. Geller, The crystal structure of brownmillerite, Ca2FeAlO5, Acta Crystallogr.Sect. B Struct. Crystallogr. Cryst. Chem. 27 (1971) 2311–2315, https://doi.org/10.1107/s056774087100579x.

[53] Q. Huang, O. Chmaissem, J.J. Capponi, C. Chaillout, M. Marezio, J.L. Tholence, A. Santoro, Neutron powder diffraction study of the crystal structure of HgBa2Ca4Cu5O12+ at room temperature and at 10 K, Phys. C Supercond.Applic. 227 (1994) 1–9, https://doi.org/10.1016/0921-4534(94)90349-2.

[54] J.C.A. Boeyens, V.V.H. Ichharam, Redetermination of the crystal structure of calcium sulphate dihydrate, CaSO4 · 2H2O, Z.Krist.New Cryst. Struct. 217 (2002) 9–10, https://doi.org/10.1524/ncrs.2002.217.jg.9.

[55] S.T. Bergold, F. Goetz-Neunhoeffer, J. Neubauer, Quantitative analysis of C-S-H in hydrating alite pastes by in-situ XRD, Cem. Concr. Res. 53 (2013) 119–126, https://doi.org/10.1016/j.cemconres.2013.06.001.

[56] S.T. Bergold, F. Goetz-Neunhoeffer, J. Neubauer, Mechanically activated alite: new insights into alite hydration, Cem. Concr. Res. 76 (2015) 202–211, https://doi.org/10.1016/j.cemconres.2015.06.005.

[57] C. Jakob, D. Jansen, U. Pott, J. Neubauer, in: Comparing Phase Development And Rheological Properties of OPC Paste Within the First Hour of Hydration, 2020, pp. 219–227, https://doi.org/10.1007/978-3-030- 22566-7_26.

[58] D.J. Morgan, D.N. Todor, Thermal Analysis of Minerals, Abacus Press, 1976, 256 pp. £12.50., Clay Miner. 13 (1978) 132–132. doi:10.1180/claymin.1978.013.1.11.

[59] J. Dweck, P.M. Buchler, A.C.V. Coelho, F.K. Cartledge, Hydration of a Portland cement blended with calcium carbonate, Thermochim. Acta 346 (2000) 105–113, https://doi.org/10.1016/S0040-6031(99)00369-X.

[60] S. Brunauer, P.H. Emmett, E. Teller, Adsorption of gases in multimolecular layers, J. Am. Chem. Soc. 60 (1938) 309–319, https://doi.org/10.1021/ja01269a023.

[61] R.M. Dreizler, E.K.U. Gross, Density Functional Theory - An Approach to the Quantum Many-body Problem, 1990.

[62] L.D. Gelb, K.E. Gubbins, R. Radhakrishnan, M. Sliwinska-Bartkowiak, Phase separation in confined systems, Rep. Prog. Phys. 62 (1999) 1573–1659, https://doi.org/10.1088/0034-4885/77/5/056502.

[63] E.P. Barrett, L.G. Joyner, P.P. Halenda, The determination of pore volume and area distributions in porous substances. I. Computations from nitrogen isotherms, J. Am. Chem. Soc. 73 (1951) 373–380, https://doi.org/10.1021/ja01145a126.

[64] Q. Yu, H.J.H. Brouwers, Gypsum: an investigation of microstructure and mechanical properties, in: G. Fischer, M. Geiker, O. Hededa, L. Ottoson, H. Stang (Eds.), Proc. 8th Fib Int. PhD Symp. Civ. Eng. Lyngby, Technical University of Denmark, 2010, pp. 341–346.

[65] C.G. Vassileva, S.V. Vassilev, Behaviour of inorganic matter during heating of Bulgarian coals, Fuel Process. Technol. 86 (2005) 1297–1333, https://doi.org/10.1016/j.fuproc.2005.01.024.

[66] A. Bakolas, E. Aggelakopoulou, A. Moropoulou, Evaluation of pozzolanic activity and physico- mechanical characteristics in ceramic powder-lime pastes, J. Therm. Anal. Calorim. 92 (2008) 345–351, https://doi.org/10.1007/s10973-007-8858-1.

[67] K. Wang, S.P. Shah, A. Mishulovich, Effects of curing temperature and NaOH addition on hydration and strength development of clinker-free CKD-fly ash binders, Cem. Concr. Res. 34 (2004) 299–309, https://doi.org/10.1016/j.cemconres.2003.08.003.

[68] Z.C. Lu, M. Haist, D. Ivanov, C. Jakob, D. Jansen, S. Leinitz, J. Link, V. Mechtcherine, J. Neubauer, J. Plank, W. Schmidt, C. Schilde, C. Schröfl, T. Sowoidnich, D. Stephan, Characterization data of reference cement CEM I 42.5 R used for priority program DFG SPP 2005 "Opus Fluidum Futurum – Rheology of reactive, multiscale, multiphase construction materials, Data Br. 27 (2019), 104699, https://doi.org/10.1016/j.dib.2019.104699.

[69] F.W. Locher, Zement - Grundlagen der Herstellung und Verwendung, Bau + Technik, Düsseldorf, 2000.

[70] E. Hering R. Martin M. Stohrer Taschenbuch der Mathematik und Physik, n.d.

[71] E. Berodier, K. Scrivener, Understanding the filler effect on the nucleation and growth of C-S-H, J. Am. Ceram. Soc. 97 (2014) 3764–3773, https://doi.org/10.1111/jace.13177.

[72] Verein Deutscher Zementwerke e.V., Zement-Taschenbuch, Verein Deutscher Zementwerke e.V., Düsseldorf, 2002.

[73] A.B. Trenwith, Thermal decomposition of isopropanol, J. Chem. Soc. Faraday Trans. 1 Phys. Chem. Condens. Phases 71 (1975) 2405–2412, https://doi.org/10.1039/F19757102405.

[74] J.W. Bullard, H.M. Jennings, R.A. Livingston, A. Nonat, G.W. Scherer, J. S. Schweitzer, K.L. Scrivener, J.J. Thomas, Mechanisms of cement hydration, Cem. Concr. Res. 41 (2011) 1208–1223, https://doi.org/10.1016/j.cemconres.2010.09.011.

[75] T. Gutberlet, Hydratation von Tricalciumsilikat – Die ersten 30 Stunden 216, 2016.

[76] C. Hesse, Der Reaktionsverlauf der frühen Hydratation von Portlandzement in Relation zur Temperatur 123, 2009, https://doi.org/10.1021/bi050862i. Dissertation.

[77] DFG SPP 2005—Priority Programm Opus Fluidum Futurum—Rheology of Reactive, Multiscale, Multiphase Construction Materials., (n.d.).